Progress In Electromagnetics Research B, Vol. 13, 433–451, 2009

SYNTHESIS OF TRIPLE-BAND AND QUAD-BAND BANDPASS FILTERS USING LUMPED-ELEMENT COPLANAR WAVEGUIDE RESONATORS

M.-S. Wu, Y.-Z. Chueh, J.-C. Yeh, and S.-G. Mao

Graduate Institute of Computer and Communication Engineering
National Taipei University of Technology
Taipei 106, Taiwan

Abstract—This paper develops a novel design method for synthesizing the multi-passband filter with high flexibility in various passband location and fractional bandwidth. Using the proposed compensation technology in the equivalent circuit of multi-passband resonator, the cutoff frequencies and matching property in passband regions can be improved. Triple- and quad-band bandpass filters operating in both wireless local area network (WLAN) 802.11 a/b/g and worldwide interoperability for microwave access (WiMAX) systems are presented to verify the design method. The lumped-element coplanar waveguide stub fabricated by the split-ring resonator is established to realize filter with compact size. All the measured, full-wave simulated and equivalent-circuit modeled results illustrate a good agreement among them, which validates the multi-passband design methodology and shows the advantages of DC elimination and deep rejection between each passband.

1. INTRODUCTION

The recent demand for multi-standard wireless and mobile communication system encourages research toward portable devices with multi-mode feature. Integrating various standards into a single wireless system with multi-band components [1–3], leading to size miniaturization and cost reduction, is an inevitable technology trend in the future. Compared with the waveguide filters in RF front-end module [4, 5], the essential multi-passband filter fabricated in printed circuit board technology provides the best candidate for multi-mode wireless mobile system due to its low profile, low cost and easy interconnection

Corresponding author: S.-G. Mao (sgmao@ieee.org).

with other components. Moreover, the passive devices using lumped elements can be realized by advanced fabrication process, such as low temperature co-fired ceramic [6] and integrated passive device [7, 8], and thus play a vital role in the development of highly integrated RF front-end module.

Numerous approaches for dual- and triple-passband filter synthesis were presented based on the techniques of frequency transformation and coupling matrix. However, most of these studies considered only the filters with specific passband response [9–13], and few researches address the method of generalized design [14–16]. However, these filters are designed to have narrow bandwidth and limited passband and stopband regions. Moreover, the dual-behavior resonator is applied to split a wide passband into multiple passbands, but the frequency response of each passband is difficult to manipulate independently [16]. With different number of passbands required for stepped-impedance resonator, the graph of design parameters, i.e., impedance and electrical length ratios, should be re-considered [12, 13].

In this study, a generalized methodology for synthesizing the multi-passband filter using lumped-element coplanar waveguide (CPW) resonator is presented. Compared to the dual-passband filter design with impedance-matching condition and phase and impedance compensation shown in authors' previous work [17], the proposed design procedure makes the inverters at each center frequency of passbands identical and thus the impedance-matching condition can be removed. Hence, it is more suitable for multi-passband filter synthesis than other previous studies [12, 13 16–18]. Moreover, the susceptance compensation is used to correct the inconsistency of frequency response of multi-passband resonator and the necessity of susceptance compensation on multi-passband filter design is verified by comparing two different filter specifications. The phase and impedance compensation are also adopted to improve the narrowband admittance inverter and to transform the impedance of multi-passband filter into characteristic impedance Z_0. Finally, the triple- and quad-passband filters operating within the wireless local area network (WLAN) 802.11 a/b/g and worldwide interoperability for microwave access (WiMAX) bands are implemented by using the novel lumped-element CPW resonators to validate the multi-passband design procedure. Therefore, the proposed design methodology is suitable for the development of multi-passband filter with controllable passband and stopband locations and different fractional bandwidths. Additionally, the presented triple- and quad-passband filters have the advantages of DC elimination, compact size, and deep rejection between each passband.

2. DESIGN METHOD

2.1. Fundamental of Multi-passband Filter Design

Figure 1(a) shows the generalized multi-passband filter network, and Fig. 1(b) indicates the multi-passband frequency response characterized by the 3-dB band-edge frequencies, $(\omega_{L1}, \omega_{H1})$, $(\omega_{L2}, \omega_{H2})$, ..., and $(\omega_{Lm}, \omega_{Hm})$, where m is the number of passband. The shunt resonator B_j in Fig. 1(a) is the multi-passband resonator shown in Fig. 2, and its input admittance can be expressed as

$$Y_{inj}^{I} = j\frac{1}{\left(\frac{\omega L_{j,1}^{I}}{\omega^2 L_{j,1}^{I} C_{j,1}^{I} - 1} + \frac{\omega L_{j,2}^{I}}{\omega^2 L_{j,2}^{I} C_{j,2}^{I} - 1} + \ldots + \frac{\omega L_{j,m}^{I}}{\omega^2 L_{j,m}^{I} C_{j,m}^{I} - 1}\right)}. \quad (1)$$

Note that the zeros of Y_{inj}^{I} associated with each resonant block in Fig. 2, i.e., $\omega_Z^{Bj,1}$, $\omega_Z^{Bj,2}$, ..., $\omega_Z^{Bj,m}$, are given by

$$\omega_Z^{Bj,i} = \frac{1}{\sqrt{L_{j,i}^{I} C_{j,i}^{I}}}, \quad \text{for } j = 1, 2, \ldots, n; \;\; i = 1, 2, \ldots, m \quad (2)$$

where n is the order of filter. When the 3-dB band-edge frequencies of the multi-passband filter, i.e., ω_{L1}, ω_{H1}, ω_{L2}, ω_{H2}, ..., ω_{Lm} and ω_{Hm},

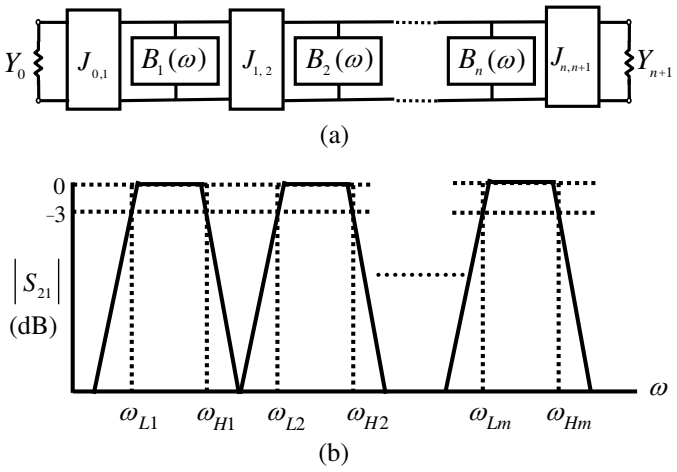

Figure 1. (a) Generalized equivalent-circuit network with admittance inverters and shunt multi-passband resonators. (b) Frequency response of the multi-passband filter.

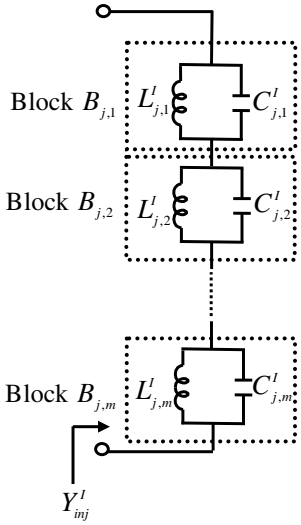

Figure 2. Equivalent multi-passband resonator with m blocks.

are given, the capacitances and inductances of the lossless equivalent multi-passband resonator can be determined by

$$C^I_{j,i} = \frac{2h}{Z_0 \omega_{ci} \Delta_i} \tag{3}$$

$$L^I_{j,i} = \frac{1}{(\omega_{ci})^2 C^I_{j,i}}, \tag{4}$$

where Z_0 is the characteristic impedance of multi-passband filter, and $\omega_{ci} = (\omega_{Li} + \omega_{Hi})/2$ and $\Delta_i = (\omega_{Hi} - \omega_{Li})/\omega_{ci}$ are the central frequency and fractional bandwidth of each passband, respectively. Note that h is a constant and can be determined arbitrarily to obtain a reasonable admittance inverter for filter implementation [19]. Moreover, the filter specification ω_{ci} is equal to $\omega_Z^{Bj,i}$, so that the elements in each block can be determined for each corresponding passband response. Furthermore, in order to examine multi-passband filter design, the equivalent network (Fig. 2) is divided into m blocks as shown in Fig. 3 and thus the corresponding input admittance for each resonant block can be obtained by

$$Y_{in}^{Bj,i} = j \frac{\omega^2 L^I_{j,i} C^I_{j,i} - 1}{\omega L^I_{j,i}}. \tag{5}$$

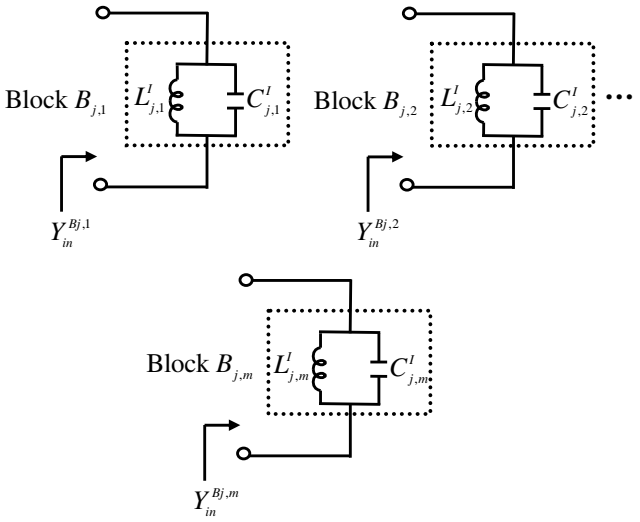

Figure 3. Individual resonant block of the equivalent multi-passband resonator shown in Fig. 2.

Regarding each passband with respect to the corresponding resonant block, the admittance inverters can be represented by [17]

$$Z^{Bi}_{Cj,j+1} = \frac{Z_0}{J^{Bi}_{j,j+1}} \tag{6}$$

$$J^{Bi}_{0,1} = \sqrt{\frac{Y_0 \Delta_i b^{Bi}_1}{g_0 g_1}}; \quad J^{Bi}_{j,j+1} = \Delta_i \sqrt{\frac{b^{Bi}_j b^{Bi}_{j+1}}{g_j g_{j+1}}}; \quad J^{Bi}_{n,n+1} = \sqrt{\frac{Y_{n+1} \Delta_i b^{Bi}_n}{g_n g_{n+1}}},$$

where

$$b^{Bi}_j = \omega^{Bj,i}_Z C^I_{j,i}. \tag{7}$$

Furthermore, let $J^{B1}_{0,1} = J^{B2}_{0,1} = \ldots = J^{Bm}_{0,1}$, $J^{B1}_{j,j+1} = J^{B2}_{j,j+1} = \ldots = J^{Bm}_{j,j+1}$ and $J^{B1}_{n,n+1} = J^{B2}_{n,n+1} = \ldots = J^{Bm}_{n,n+1}$, then

$$\Delta_1 b^{B1}_j = \Delta_2 b^{B2}_j = \ldots = \Delta_m b^{Bm}_j = \frac{2h}{Z_0}, \tag{8}$$

which indicates that the impedance matching condition can be achieved at central passband frequency ω_{ci}. The length of admittance inverter is $\lambda_g/4$ at central stopband frequency $\omega_P = \frac{\omega_{c1}+\omega_{cm}}{2}$, where λ_g is the guided wavelength. However, the frequency response of the input admittance in each resonant block, i.e., $Y^{Bj,1}_{in}$, $Y^{Bj,2}_{in}$, $\ldots$, $Y^{Bj,m}_{in}$,

may not coincide with that of the whole equivalent multi-passband resonator Y_{inj}^{I} at each individual passband region, which leads to the discrepancy in each passband bandwidth. Hence, the susceptance compensation is proposed to improve the deviation.

2.2. Susceptance Compensation

Following the above design procedure, the multi-passband resonator gives $Y_{in}^{Bj,i} = Y_{inj}^{I}$ at ω_{ci}. However, the frequency response of the equivalent circuit of multi-passband resonator shown in Fig. 2 is not equal to the passband region of the individual resonant block (Fig. 3), and thus Eq. (1) is not identical to Eq. (5) at the frequency of interest: (ω_{L1}, ω_{H1}) for the first passband, (ω_{L2}, ω_{H2}) for the second passband, ..., and (ω_{Lm}, ω_{Hm}) for the m-th passband, which shows that the discrepancy is occurred between the design and specification. Accordingly, the susceptance compensation to correct the deviation is presented by equating Y_{inj}^{I} to $Y_{in}^{Bj,i}$ at each 3-dB band-edge frequency, and thus we have

$$\frac{1}{\left(\frac{\omega_{Li}L_{j,1P}^{I}}{\omega_{Li}^{2}L_{j,1P}^{I}C_{j,1P}^{I}-1}+\frac{\omega_{Li}L_{j,2P}^{I}}{\omega_{Li}^{2}L_{j,2P}^{I}C_{j,2P}^{I}-1}+\ldots+\frac{\omega_{Li}L_{j,mP}^{I}}{\omega_{Li}^{2}L_{j,mP}^{I}C_{j,mP}^{I}-1}\right)}=Y_{inL}^{B_{j,i}} \quad (9)$$

$$\frac{1}{\left(\frac{\omega_{Hi}L_{j,1P}^{I}}{\omega_{Hi}^{2}L_{j,1P}^{I}C_{j,1P}^{I}-1}+\frac{\omega_{Hi}L_{j,2P}^{I}}{\omega_{Hi}^{2}L_{j,2P}^{I}C_{j,2P}^{I}-1}+\ldots+\frac{\omega_{Hi}L_{j,mP}^{I}}{\omega_{Hi}^{2}L_{j,mP}^{I}C_{j,mP}^{I}-1}\right)}=Y_{inH}^{B_{j,i}} \quad (10)$$

where

$$Y_{inL}^{B_{j,i}}=\frac{\omega_{Li}^{2}L_{j,i}^{I}C_{j,i}^{I}-1}{\omega_{Li}L_{j,i}^{I}}$$

$$Y_{inH}^{B_{j,i}}=\frac{\omega_{Hi}^{2}L_{j,i}^{I}C_{j,i}^{I}-1}{\omega_{Hi}L_{j,i}^{I}}\ .$$

The iterative process is used to determine $L_{j,iP}^{I}$ and $C_{j,iP}^{I}$ based on (9) and (10). Hence, the susceptance compensation condition is satisfied and consequently the equivalence of input admittances $Y_{inj}^{I} = Y_{in}^{Bj,i}$ is established at each 3-dB band-edge frequency.

2.3. Phase and Impedance Compensation

To improve the narrowband property of admittance inverter and to transform the impedance of multi-passband filter to Z_0 at each

central passband frequency, the phase and impedance compensation are applied by adding the following capacitances into the corresponding multi-passband resonators [17]:

$$C_{0,1}^{Bi} = \frac{1 - \sin\left(\omega_Z^{B1,i}\pi/2\omega_P\right)}{\omega_Z^{B1,i} Z_{C0,1}^{Bi} \cos\left(\omega_Z^{B1,i}\pi/2\omega_P\right)} \tag{11}$$

$$C_{j,j+1}^{Bi} = \frac{\cos\left(\omega_Z^{Bj+1,i}\pi/2\omega_P\right)}{\omega_Z^{Bj+1,i} Z_{Cj,j+1}^{Bi} \sin\left(\omega_Z^{Bj+1,i}\pi/2\omega_P\right)} \tag{12}$$

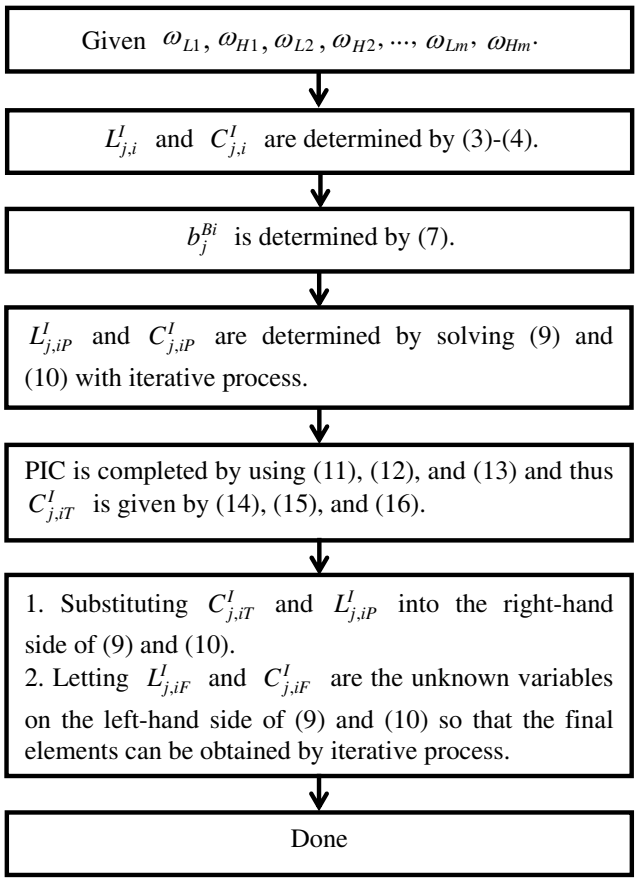

Figure 4. Complete flowchart of multi-passband filter design methodology. Phase and impedance compensation: PIC.

$$C_{n,n+1}^{Bi} = \frac{1 - \sin\left(\omega_Z^{Bn,i}\pi/2\omega_P\right)}{\omega_Z^{Bn,i} Z_{Cn,n+1}^{Bi} \cos\left(\omega_Z^{Bn,i}\pi/2\omega_P\right)}. \tag{13}$$

Then the total capacitances in each resonant block can be obtained, respectively,

$$C_{1,iT}^{I} = C_{1,iP}^{I} + C_{0,1}^{Bi} + C_{1,2}^{Bi} \tag{14}$$

$$C_{j+1,iT}^{I} = C_{j+1,iP}^{I} + 2C_{j,j+1}^{Bi} \tag{15}$$

$$C_{n,iT}^{I} = C_{n,iP}^{I} + C_{n-1,n}^{Bi} + C_{n,n+1}^{Bi}. \tag{16}$$

Figure 4 depicts the complete design flowchart of the multi-passband filter synthesis methodology, and the equivalent network of multi-passband filter is illustrated in Fig. 5. However, because the phase and impedance compensation deal mainly with the admittance inverter by regarding each resonant block independently, the susceptance compensation presented in Fig. 4 should be applied again, so that the final inductance $L_{j,iF}^{I}$ and capacitance $C_{j,iF}^{I}$ are determined.

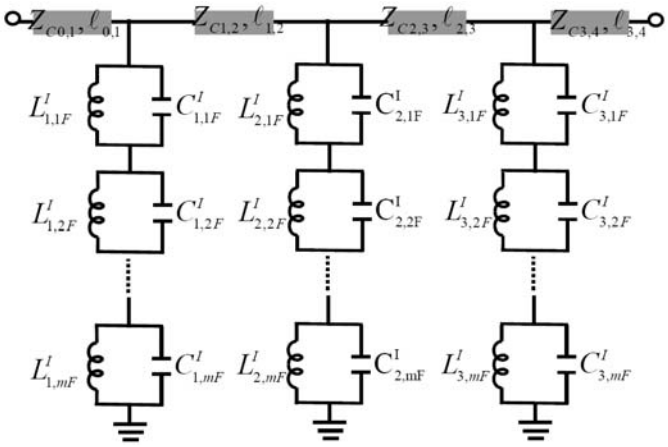

Figure 5. Equivalent-circuit model of the 3rd-order multi-passband filter.

To validate the necessity of compensation technology, two multi-passband filters with significantly different specifications are presented for comparison. Cases I and II are the quad-passband responses with various passband locations and operating bandwidths. The calculated results of third-order Chebyshev quad-passband filters with

and without compensation, i.e., susceptance compensation and phase and impedance compensation, are shown in Tables 1 and 2. The results indicate that the design procedure with compensation meets the given specification, and thus verify the requirement of the compensation technique in multi-passband filter design procedure. Moreover, the presented two cases with completely different filter specifications demonstrate that the proposed design methodology is suitable for filters with flexible passband location and fractional bandwidth.

3. FILTER IMPLEMENTATION

In this section, the 3rd-order Chebyshev triple- and quad-passband filters with 0.1-dB ripple response are realized for WLAN and WiMAX applications. All the circuits in this study are fabricated on RT/Duroid 6010 substrate with 1-oz copper cladding, 0.635 mm substrate thickness, and the dielectric constant of 10.2. The full-wave simulator IE3D is used to investigate the proposed multi-passband filters. The lowpass filter prototype, normalizing the cut-off frequency to 3-dB band-edge point, can be determined $g_0 = g_4 = 1$, $g_1 = 1.4367$, $g_2 = 1.598$, and $g_3 = 1.4367$ [20]. Moreover, the value h is typically in the range $0 < h \leq 1$ [19]. In this study, this constant h is chosen as 0.39 for better matching property in each passband. Moreover, in order to realize the equivalent multi-passband resonator, the series-connected shunt LC resonators in Fig. 5 are transformed into the conventional

Table 1. 3-dB band-edge frequency points of 3rd-order Chebyshev quad-passband filter with and without compensation for case I.

Frequency	Specification	With Compensation	Without Compensation
f_{L1}	2 GHz	2.07 GHz	2.17 GHz
f_{H1}	2.5 GHz	2.52 GHz	2.52 GHz
f_{L2}	2.7 GHz	2.68 GHz	2.79 GHz
f_{H2}	3 GHz	2.93 GHz	3.18 GHz
f_{L3}	5.1 GHz	5.15 GHz	5 GHz
f_{H3}	5.4 GHz	5.42 GHz	5.32 GHz
f_{L4}	5.6 GHz	5.57 GHz	5.63 GHz
f_{H4}	6.2 GHz	6.13 GHz	6 GHz

Table 2. 3-dB band-edge frequency points of 3rd-order Chebyshev quad-passband filter with and without compensation for case II.

Frequency	Specification	With Compensation	Without Compensation
f_{L1}	2 GHz	2.02 GHz	2.17 GHz
f_{H1}	2.5 GHz	2.52 GHz	2.62 GHz
f_{L2}	3.7 GHz	3.74 GHz	3.72 GHz
f_{H2}	4 GHz	4.02 GHz	3.97 GHz
f_{L3}	4.2 GHz	4.19 GHz	4.24 GHz
f_{H3}	4.5 GHz	4.43 GHz	4.5 GHz
f_{L4}	5.6 GHz	5.57 GHz	5.56 GHz
f_{H4}	6.2 GHz	6.2 GHz	6 GHz

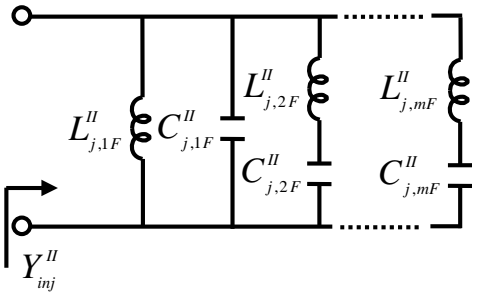

Figure 6. Conventional multi-passband resonator.

multi-passband resonator in Fig. 6 with the input admittance

$$Y^{II}_{inj} = j\left(\frac{\omega^2 C^{II}_{j,1F} L^{II}_{j,1F} - 1}{\omega L^{II}_{j,1F}} - \frac{\omega C^{II}_{j,2F}}{\omega^2 C^{II}_{j,2F} L^{II}_{j,2F} - 1} - \ldots - \frac{\omega C^{II}_{j,mF}}{\omega^2 C^{II}_{j,mF} L^{II}_{j,mF} - 1}\right). \quad (17)$$

3.1. Triple-passband Filter

The frequency specification of the triple-passband filter applicable to WLAN 802.11 a/b/g and WiMAX bands is $f_{L1} = 1.9\,\text{GHz}$, $f_{H1} = 2.7\,\text{GHz}$, $f_{L2} = 3.35\,\text{GHz}$, $f_{H2} = 3.7\,\text{GHz}$, $f_{L3} = 4.9\,\text{GHz}$ and $f_{H3} = 5.8\,\text{GHz}$, and the fractional bandwidths of three passbands are

$\Delta_1 = 34.8\%$, $\Delta_2 = 10\%$ and $\Delta_3 = 16.8\%$. Moreover, in order to easily realize the triple-passband filter, the equivalent triple-passband resonator (Fig. 2) is transformed into the conventional resonator (Fig. 6) by using the following equations:

$$C^{II}_{j,1F} = \frac{a}{d} \tag{18}$$

$$L^{II}_{j,1F} = f \tag{19}$$

$$C^{II}_{j,2F} = \frac{cg^2 - g^3 - bg + a}{fg^2 - d} \tag{20}$$

$$L^{II}_{j,2F} = \frac{g}{C^{II}_{j,2F}} \tag{21}$$

$$C^{II}_{j,3F} = \frac{cdfg - dfg^2 - f^2ga - d^2}{f^2dg} - C^{II}_{j,2F} \tag{22}$$

$$L^{II}_{j,3F} = \frac{d}{C^{II}_{j,3F}fg} \tag{23}$$

where

$$\begin{aligned}
a &= L^I_{j,1F}C^I_{j,1F}L^I_{j,2F}C^I_{j,2F}L^I_{j,3F}C^I_{j,3F} \\
b &= L^I_{j,1F}C^I_{j,1F}L^I_{j,2F}C^I_{j,2F}L^I_{j,3F}C^I_{j,3F} \\
&\quad \times \left(\frac{1}{L^I_{j,1F}C^I_{j,1F}} + \frac{1}{L^I_{j,2F}C^I_{j,2F}} + \frac{1}{L^I_{j,3F}C^I_{j,3F}}\right) \\
c &= L^I_{j,1F}C^I_{j,1F} + L^I_{j,2F}C^I_{j,2F} + L^I_{j,3F}C^I_{j,3F} \\
d &= L^I_{j,1F}C^I_{j,1F}L^I_{j,2F}C^I_{j,2F}L^I_{j,3F}C^I_{j,3F}\left(\frac{1}{C^I_{j,1F}} + \frac{1}{C^I_{j,2F}} + \frac{1}{C^I_{j,3F}}\right)
\end{aligned}$$

$$\begin{aligned}
e &= L^I_{j,1F}C^I_{j,1F}\left(L^I_{j,2F} + L^I_{j,3F}\right) + L^I_{j,2F}C^I_{j,2F}\left(L^I_{j,1F} + L^I_{j,3F}\right) \\
&\quad + L^I_{j,3F}C^I_{j,3F}\left(L^I_{j,1F} + L^I_{j,2F}\right) \\
f &= L^I_{j,1F} + L^I_{j,2F} + L^I_{j,3F} \\
g &= \frac{e + \sqrt{e^2 - 4df}}{2f}.
\end{aligned}$$

The calculated LC elements of the conventional triple-passband resonator for the triple-passband filter are given in Table 3.

To verify the design method, the novel lumped-element CPW stub is used to implement the triple-passband filter. Fig. 7(a) depicts the

physical configuration of the resonator and its corresponding equivalent circuit. The behavior of the open stub is equivalent to the series $L_{s1}C_{s1}$ resonator and two neighboring symmetric split-ring resonators (SRRs) can be modeled by the shunt $L_{SRR}C_{SRR}$ resonator [21]. Then the equivalent circuit can be transformed into two series $L'_{s1}C'_{s1}$ and $L'_{s2}C'_{s2}$ resonators in parallel connection [22]. Moreover, the lumped-element CPW stub shown in Fig. 7(b) can be modeled as the parallel-connected L_{p1} inductor and series L_tC_{p1} resonator[23]. Thanks to the parasitic inductance L_t is quite low at lower frequency, the circuits shown in Figs. 7(a) and (b) are connected in parallel to exhibit the conventional triple-passband resonator network. Hence, the required slope of the input admittance can be achieved by fitting the equivalent-

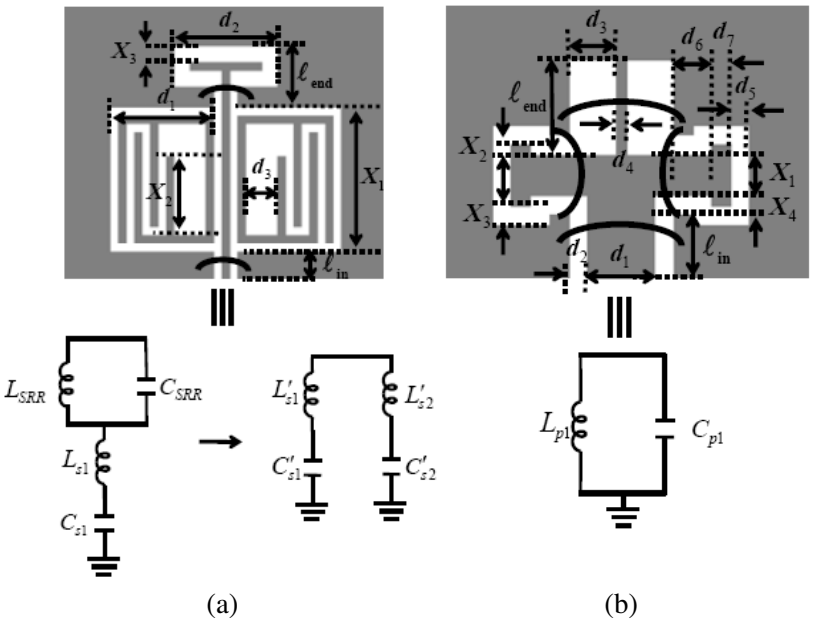

Figure 7. (a) Geometry and the corresponding equivalent circuit of the lumped-element CPW stub for triple-passband filter ($d_1 = 2.4\,\text{mm}$, $d_2 = 2.6\,\text{mm}$, $d_3 = 0.8\,\text{mm}$, $X_1 = 3.5\,\text{mm}$, $X_2 = 1.9\,\text{mm}$, $X_3 = 0.4\,\text{mm}$, $\ell_{in} = 1\,\text{mm}$, $\ell_{end} = 1.5\,\text{mm}$. All the other strip and slot widths are $0.2\,\text{mm}$). (b) Geometry and the corresponding equivalent circuit of the lumped-element CPW stub for triple-passband filter ($d_1 = 1.4\,\text{mm}$, $d_2 = 0.4\,\text{mm}$, $d_3 = 1\,\text{mm}$, $d_4 = 0.2\,\text{mm}$, $d_5 = 0.4\,\text{mm}$, $d_6 = 0.8\,\text{mm}$, $d_7 = 0.4\,\text{mm}$, $X_1 = 0.8\,\text{mm}$, $X_2 = 0.2\,\text{mm}$, $X_3 = X_4 = 0.4\,\text{mm}$, $\ell_{in} = 1.3\,\text{mm}$, $\ell_{end} = 1.9\,\text{mm}$).

circuit model to a full-wave simulation as shown in Fig. 8(a). Note that an additional pole at around 7.4 GHz in full-wave simulation is due to the parasitic series resonance caused by the series L_tC_{p1} resonator at higher frequency[23].

The physical construction of the triple-passband filter is presented in Fig. 8(b). Fig. 9 depicts the triple-passband responses, which demonstrates a very good agreement among the measured, full-wave simulated, and equivalent-circuit modeled results. The measured frequency limits are observed at $f_{L1} = 2.08\,\text{GHz}$, $f_{H1} = 2.58\,\text{GHz}$, $f_{L2} = 3.32\,\text{GHz}$, $f_{H2} = 3.69\,\text{GHz}$, $f_{L3} = 4.85\,\text{GHz}$ and $f_{H3} = 5.82\,\text{GHz}$, which closely meets the filter specification and thus verifies the proposed design methodology. Additionally, the measured insertion losses of the in-band central frequencies are better than 0.75, 1.53, and 1.4 dB at 2.34, 3.5, and 5.3 GHz, respectively. The deep suppression at 2.8 and 4.25 GHz is attributed to the resonance of the CPW stub shown in Fig. 7(a), which is regardless of the multi-passband filter design. Moreover, the discrepancy between the equivalent circuit and measurement at around 7.5 GHz is mainly caused by the existing pole in the input susceptance of full-wave simulation as depicted in Fig. 8(a).

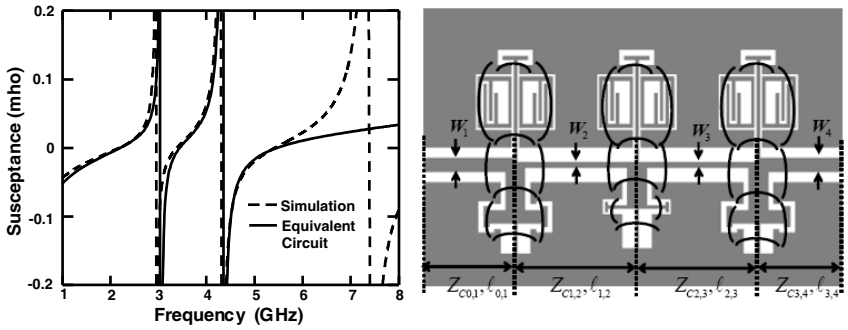

(a) (b)

Figure 8. (a) Input susceptance of the lumped-element CPW stub by shunt connecting structures of Figs. 7(a) and (b). (b) Geometry of the triple-passband filter with $W_1 = W_4 = 0.8\,\text{mm}$, $W_2 = W_3 = 0.28\,\text{mm}$, $\ell_{0,1} = \ell_{4,3} = 9.4\,\text{mm}$, $\ell_{1,2} = \ell_{2,3} = 8.8\,\text{mm}$. (For the central CPW stub, the dimensions shown in Fig. 7(b) are $d_1 = 1.4\,\text{mm}$, $d_2 = 0.4\,\text{mm}$, $d_3 = 1\,\text{mm}$, $d_4 = 0.2\,\text{mm}$, $d_5 = 0.2\,\text{mm}$, $d_6 = 1\,\text{mm}$, $d_7 = 0.2\,\text{mm}$, $X_1 = 0.2\,\text{mm}$, $X_2 = 0.2\,\text{mm}$, $X_3 = X_4 = 0.4\,\text{mm}$, $\ell_{in} = 1\,\text{mm}$, $\ell_{end} = 2.5\,\text{mm}$; The dimensions of the other stubs are the same as in Figs. 7(a) and (b)).

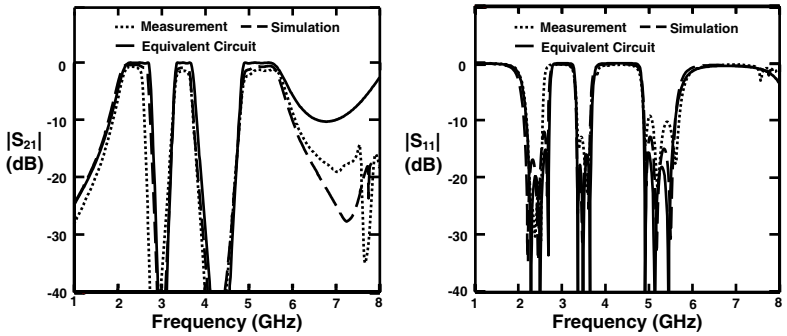

Figure 9. Measured, full-wave simulated, and equivalent-circuit modeled S-parameters of the triple-passband filter.

Table 3. Equivalent circuit elements of 3rd-order Chebyshev multi-passband filter using the conventional multi-passband resonator.

Elements	Triple-Passband Filter	Quad-Passband Filter
$Z_{C0,1} = Z_{C3,4}$	67.8587 ohm	67.8587 ohm
$Z_{C1,2} = Z_{C2,3}$	97.1285 ohm	97.1285 ohm
$L^{II}_{11F} = L^{II}_{31F}$	2.5386 nH	2.6754 nH
$C^{II}_{11F} = C^{II}_{31F}$	1.0061 pF	0.74 pF
$L^{II}_{12F} = L^{II}_{32F}$	9.4317 nH	9.6324 nH
$C^{II}_{12F} = C^{II}_{32F}$	0.2888 pF	0.162 pF
$L^{II}_{13F} = L^{II}_{33F}$	4.1771 nH	12.5516 nH
$C^{II}_{13F} = C^{II}_{33F}$	0.3234 pF	0.219 pF
$L^{II}_{14F} = L^{II}_{34F}$	-	9.609 nH
$C^{II}_{14F} = C^{II}_{34F}$	-	0.1024 pF
L^{II}_{21F}	2.7614 nH	3.0185 nH
C^{II}_{21F}	0.9189 pF	0.6424 pF
L^{II}_{22F}	8.9575 nH	9.4906 nH
C^{II}_{22F}	0.3072 pF	0.1653 pF
L^{II}_{23F}	4.0416 nH	12.1792 nH
C^{II}_{23F}	0.3359 pF	0.2278 pF
L^{II}_{24F}	-	9.2613 nH
C^{II}_{24F}	-	0.1065 pF

3.2. Quad-passband Filter

The specification for the quad-passband filter is given by $f_{L1} = 2\,\text{GHz}$, $f_{H1} = 2.8\,\text{GHz}$, $f_{L2} = 3.35\,\text{GHz}$, $f_{H2} = 3.7\,\text{GHz}$, $f_{L3} = 4.35\,\text{GHz}$, $f_{H3} = 4.7\,\text{GHz}$, $f_{L4} = 5.4\,\text{GHz}$ and $f_{H4} = 6.5\,\text{GHz}$. The bandwidths of the corresponding passbands are $\Delta_1 = 33.3\%$, $\Delta_2 = 10\%$, $\Delta_3 = 7.7\%$ and $\Delta_4 = 18.5\%$, respectively. To implement the quad-passband filter, the equivalent quad-passband resonator (Fig. 2) is transformed to the resonant circuit shown in Fig. 6 to obtain the corresponding LC elements given in Table 3.

Figure 10 indicates the lumped-element CPW stubs and their corresponding equivalent circuits. Hence, the input susceptance of the shunt resonator used in filter design can be obtained by

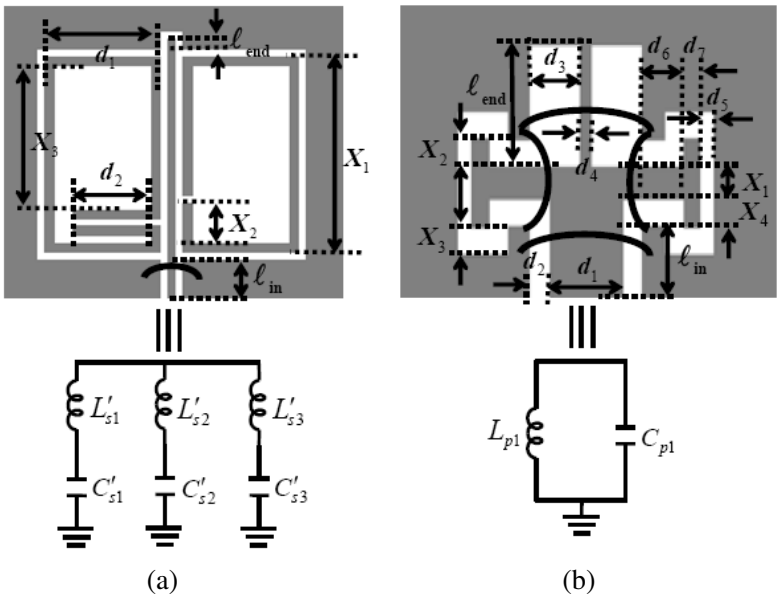

Figure 10. (a) Geometry and the corresponding equivalent circuit of the lumped-element CPW stub for quad-passband filter. ($d_1 = 2.8\,\text{mm}$, $d_2 = 1.8\,\text{mm}$, $X_1 = 4.7\,\text{mm}$, $X_2 = 0.95\,\text{mm}$, $X_3 = 3.5\,\text{mm}$, $\ell_{in} = 1\,\text{mm}$, $\ell_{end} = 0.2\,\text{mm}$. All the other strip and slot widths are $0.2\,\text{mm}$). (b) Geometry and the corresponding equivalent circuit of the lumped-element CPW stub for quad-passband filter ($d_1 = 1.4\,\text{mm}$, $d_2 = 0.4\,\text{mm}$, $d_3 = 1\,\text{mm}$, $d_4 = 0.2\,\text{mm}$, $d_5 = 0.4\,\text{mm}$, $d_6 = 0.8\,\text{mm}$, $d_7 = 0.2\,\text{mm}$, $X_1 = X_2 = X_3 = X_4 = 0.4\,\text{mm}$, $\ell_{in} = 1\,\text{mm}$, $\ell_{end} = 1.7\,\text{mm}$).

parallel connecting the circuits shown in Figs. 10(a) and (b). The element values in the equivalent-circuited model are determined by satisfying the full-wave simulation as shown in Fig. 11(a). Accordingly, the physical configuration of the quad-passband filter presented in Fig. 11(b) can be realized. As shown in Fig. 12, the measured in-band insertion losses are 0.68, 2.05, 1.94, and 1.58 dB at 2.45, 3.47, 4.43, and 5.81 GHz, respectively, and the measured frequency limits are $f_{L1} = 2.17\,\text{GHz}$, $f_{H1} = 2.72\,\text{GHz}$, $f_{L2} = 3.33\,\text{GHz}$, $f_{H2} = 3.61\,\text{GHz}$, $f_{L3} = 4.26\,\text{GHz}$, $f_{H3} = 4.6\,\text{GHz}$, $f_{L4} = 5.35\,\text{GHz}$ and $f_{H4} = 6.26\,\text{GHz}$. The full-wave simulated and equivalent-circuit modeled S-parameters are also included in Fig. 12 to reveal a very good agreement among them.

Note that discrepancy between the measurement and full-wave simulation is due to the fabrication tolerance in the physical dimension and bonding wires. Additionally, the insertion loss increases inevitably when the passband bandwidth becomes quite narrow. The sizes of the presented triple- and quad-passband filters are both approximately $\lambda_g \times 0.33\lambda_g$ at ω_P.

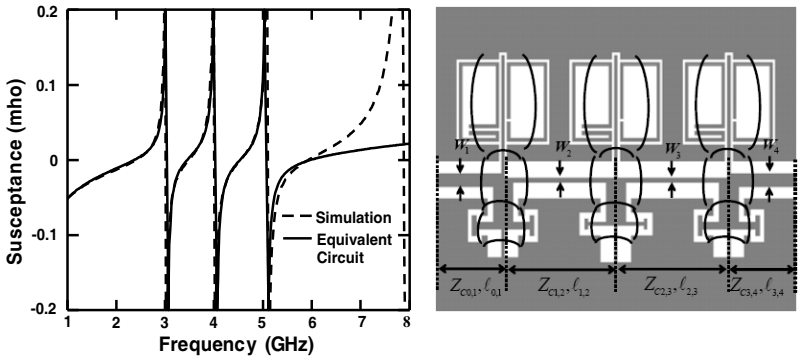

Figure 11. (a) Calculated input susceptance of the lumped-element CPW by shunt connecting structures of Figs. 10(a) and (b). (b) Geometry of the quad-passband filter with $W_1 = W_4 = 0.8\,\text{mm}$, $W_2 = W_3 = 0.28\,\text{mm}$, $\ell_{0,1} = \ell_{4,3} = 8.8\,\text{mm}$, $\ell_{1,2} = \ell_{2,3} = 8\,\text{mm}$. (For the central CPW stub, the dimensions shown in Fig. 10(b) are $d_1 = 1.4\,\text{mm}$, $d_2 = 0.4\,\text{mm}$, $d_3 = 1\,\text{mm}$, $d_4 = 0.2\,\text{mm}$, $d_5 = 0.4\,\text{mm}$, $d_6 = 0.9\,\text{mm}$, $d_7 = 0.3\,\text{mm}$, $X_1 = X_2 = 0.2\,\text{mm}$, $X_3 = 0.4\,\text{mm}$, $X_4 = 0.6\,\text{mm}$, $\ell_{in} = 0.8\,\text{mm}$, $\ell_{end} = 2.2\,\text{mm}$; The dimensions of the other stubs are the same as in Figs. 10(a) and (b)).

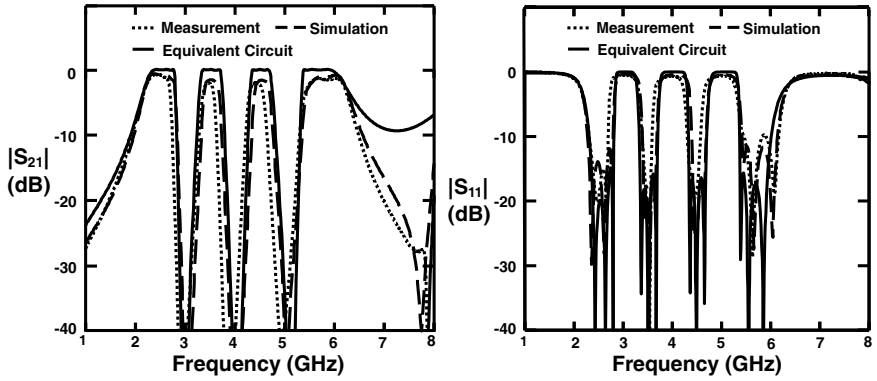

Figure 12. Measured, full-wave simulated, and equivalent-circuit modeled S-parameters of the quad-passband filter.

4. CONCLUSION

A general synthesis technique for novel multi-passband filter has been presented in this study. Contrary to the authors' previous work [17], the proposed design methodology uses the newly developed susceptance compensation technique to further improve the performance of multi-passband filter. Moreover, the passband response is easily controlled and thus the design procedure is suitable for versatile filter applications. Two multi-passband filters, i.e., triple- and quad-band bandpass filters, are established to validate the flexibility of design procedure for different filter specifications. The equivalent circuits of the filters are constructed based on susceptance and phase and impedance compensation, and the transformation equation is applied to obtained lumped-element CPW stub for practical feasibility. Therefore, the physical configuration of the multi-passband filters operating in both WLAN 802.11 a/b/g and WiMAX systems can be realized. The measured, full-wave simulated, and equivalent-circuit modeled results show that the impedance matching can be achieved at each operating passband and the unwanted DC is suppressed in the lower frequency region. Furthermore, the proposed design procedure with compensation technology can be further developed to design other multi-band components, such as multi-band baluns and couplers, and this exploration will be presented in the near future.

REFERENCES

1. Chen, X.-P., K. Wu, and Z.-L. Li, "Dual-band and triple-band substrate integrated waveguide filters with Chebyshev and quasi-elliptic responses," *IEEE Trans. Microw. Theory Tech.*, Vol. 55, No. 12, 2569–2578, December 2007.
2. Cheng, K.-K. M. and C. Law, "A new approach to the realization of a dual-band microstrip filter with very wide upper stopband," *IEEE Trans. Microw. Theory Tech.*, Vol. 56, No. 6, 1461–1467, June 2008.
3. Gao, X., L. K. Yeung, and K.-L. Wu, "A dual-band balun using partially coupled stepped-impedance coupled-line resonators," *IEEE Trans. Microw. Theory Tech.*, Vol. 56, No. 6, 1455–1460, June 2008.
4. Lee, J., M. S. Uhm, and I.-B. Yom, "A dual-passband filter of canonical structure for satellite applications," *IEEE Microw. Wireless Compon. Lett.*, Vol. 14, No. 6, 271–273, June 2004.
5. Amari, S. and M. Bekheit, "A new class of dual-mode dual-band waveguide filters," *IEEE Trans. Microw. Theory Tech.*, Vol. 56, No. 8, 1938–1944, August 2008.
6. Lee, Y. C., "CPW-to-stripline vertical via transitions for 60 GHz Ltcc sop applications," *Progress In Electromagnetics Research Letters*, Vol. 2, 37–44, 2008.
7. Zoschke, K., J. Wolf, M. Topper, O. Ehrmann, T. Fritzsch, K. Scherpinski, H. Reichl, and F.-J. Schmuckle, "Thin film integration of passive — Single components, filters, integrated passive devices," *IEEE Proceedings of 54th Electronic Components and Technology Conference*, 294–301, Las Vegas, NV, June 2004.
8. Liu, L., S.-M. Kuo, J. Abrokwah, M. Ray, D. Maurer, and M. Miller, "Compact harmonic filter design and fabrication using IPD technology," *IEEE Trans. Microw. Theory Tech.*, Vol. 30, No. 12, 556–562, December 2007.
9. Wang, X.-H. and B.-Z. Wang, "Compact broadband dual-band bandpass filters using slotted ground structures," *Progress In Electromagnetics Research*, PIER 82, 151–166, 2008.
10. Fan, J.-W., C.-H. Liang, and X.-W. Dai, "Design of cross-coupled dual-band filter with equal-length split-ring resonators," *Progress In Electromagnetics Research*, PIER 75, 285–293, 2007.
11. Lee, J. and K. Sarabandi, "Design of triple-passband microwave filters using frequency transformations," *IEEE Trans. Microw. Theory Tech.*, Vol. 56, No. 1, 187–193, January 2008.
12. Chen, C.-F., T.-Y. Huang, and R.-B. Wu, "Design of dual-

and triple-passband filters using alternately cascaded multiband resonators," *IEEE Trans. Microw. Theory Tech.*, Vol. 54, No. 9, 3550–3558, September 2006.

13. Kuo, J.-T., T.-H. Yeh, and C.-C. Yeh, "Design of microstrip bandpass filters with a dual-passband response," *IEEE Trans. Microw. Theory Tech.*, Vol. 53, No. 4, 1331–1337, April 2005.
14. Zhang, Y., K. A. Zaki, J. A. Ruiz-Cruz, and A. E. Atia, "Analytical synthesis of generalized multi-band microwave filters," *IEEE MTT-S Int. Microwave Symp. Dig.,* 1273–1276, June 2007.
15. Lunot, V., S. Bila, and F. Seyfert, "Optimal synthesis for multi-band microwave filters," *IEEE MTT-S Int. Microwave Symp. Dig.*, 115–118, June 2007.
16. Quendo, C., A. Manchec, Y. Clavet, E. Rius, J.-F. Favennec, and C. Person, "General synthesis of n-band resonator based on n-order dual behavior resonator," *IEEE Microw. Wireless Compon. Lett.*, Vol. 17, No. 5, 337–339, May 2007.
17. Mao, S.-G. and M.-S. Wu, "Design of artificial lumped-element coplanar waveguide filters with controllable dual-passband responses," *IEEE Trans. Microw. Theory Tech.*, Vol. 56, No. 7, 1684–1692, July 2008.
18. Mao, S.-G., M.-S. Wu, and Y.-Z. Chueh, "Design of composite right/left-handed coplanar-waveguide bandpass and dual-passband filters," *IEEE Trans. Microw. Theory Tech.*, Vol. 54, No. 9, 3543–3549, September 2006.
19. Matthaei, G., L. Young, and E. M. T. Jones, *Microwave Filter, Impedance-matching Networks, and Coupling Structures*, 595–605, Artech House, Norwood, MA, 1980.
20. Williams, A. B. and F. J. Taylor, *Electronic Filter Design Handbook*, 3rd edition, 2.36–2.43, McGraw-Hill, 1995.
21. Baena, J. D., J. Bonache, F. Martin, R. M. Sillero, F. Falcone, T. Lopetegi, M. A. G. Laso, J. Garcia-Garcia, I. Gil, M. F. Portillo, and M. Sorolla, "Equivalent-circuit models for split-ring resonators and complementary split-ring resonators coupled to planar transmission lines," *IEEE Trans. Microw. Theory Tech.*, Vol. 53, No. 4, 1451–1461, April 2005.
22. Hong, J. S. and M. J. Lancaster, *Microstrip Filters for RF/Microwave Applications*, Wiley, New York, 2001.
23. Mao, S.-G. and Y.-Z. Chueh, "Compact dual-passband filter using lumped-element coplanar waveguide resonators," *Electron. Lett.*, Vol. 43, No. 16, 873–875, August 2, 2007.